Impact of bioreactor process parameters and yeast biomass on Raman spectra

Klaverdijk, Maarten; Nemati, Mehrab; Ottens, Marcel; Klijn, Marieke E.

DOI
10.1002/btpr.70050

Publication date
2025

Document Version
Final published version

Published in
Biotechnology Progress

Received: 10 March 2025 | Revised: 30 May 2025 | Accepted: 6 June 2025

DOI: 10.1002/btpr.70050

BIOTECHNOLOGY PROGRESS

RESEARCH ARTICLE

Process Sensing and Control

Impact of bioreactor process parameters and yeast biomass on Raman spectra

Maarten Klaverdijk | Mehrab Nemati | Marcel Ottens | Marieke E. Klijn

Department of Biotechnology, Delft University of Technology, Delft, The Netherlands

Correspondence
Marieke E. Klijn, Department of Biotechnology, Delft University of Technology, Van der Maasweg 9, Delft, 2629 HZ, The Netherlands.
Email: m.e.klijn@tudelft.nl

Funding information
Department of Biotechnology at Delft University of Technology

Abstract

In-line Raman spectroscopy combined with chemometric modeling is a valuable process analytical technology (PAT) providing real-time quantitative information on cell culture compounds. Considering that compound quantification through chemometric models depends on pre-processing to maintain consistent changes in intensity at certain wavenumbers, all causes of signal distortion should be well understood to prevent quantification inaccuracies. This work investigated spectral distortion caused by the changing bioreactor parameters temperature, bubble quantity, and medium viscosity. In addition, the isolated spectral contribution of *Saccharomyces cerevisiae* cells in suspension was also determined. A temperature range from 20 to 40°C resulted in peak shifts up to 0.8 cm^{-1} to lower wavenumbers, bubbles generated under standard bioreactor operation conditions led to signal attenuation of up to 7.93% reduction in peak intensity, and changes in liquid viscosity resulted in complex peak shift behavior. Isolated biomass concentrations reaching 5 g/L caused up to 44.6% reduction in distinct peak intensity, which was similar to spectra from batch process fermentations. Correcting for the attenuation revealed spectral features of biomass associated with proteins and lipids in the 1000–1500 cm^{-1} region. However, the spectral contribution of yeast biomass is dominated by signal extinction, which attenuates Raman spectra in a non-linear manner as biomass accumulates. The obtained knowledge on different sources of spectral distortion aids in the development of robust pre-processing and modeling strategies to obtain chemometric models applicable across experimental setups.

KEYWORDS
in-line measurements, process analytical technology, Raman spectroscopy, real-time monitoring, *Saccharomyces cerevisiae*, spectral pre-processing

1 | INTRODUCTION

Monitoring the progression of substrate, product, and biomass concentration in bioprocesses is traditionally measured off-line. This means that a physical sample is manually taken from the system and analyzed by using an external standalone machine. Off-line measurements are labor-intensive and severely limit the real-time resolution of monitoring a process. Furthermore, manual sampling is invasive and increases the risk of altering or contaminating the process. The process analytical technology (PAT) framework published in 2004[1]

addressed these issues and aims to improve process understanding and control through real-time monitoring strategies. The PAT initiative and eased regulatory acceptance toward new analytical tools led to an increase in research and application of real-time monitoring strategies.[2]

Optical spectroscopy PAT offers non-invasive and non-destructive measurement methods and can be placed in-line to the bioreactor allowing direct measurements, thereby lowering the risk of contamination.[3] Of the available spectroscopic tools, Raman spectroscopy is especially suitable for bioreactor environments due to the low signal interference from water. It also enables measurements through glass interfaces, facilitating easy integration with closed systems.[4] Raman spectroscopy is based on measuring inelastically scattered light coming from the interaction between monochromatic light and molecules in the sample. Each molecule provides a unique pattern of peaks based on the vibrational modes in the molecule's structure (Raman fingerprint), making Raman a powerful analytical tool for analyzing specific targets of interest. Furthermore, there is a linear correlation between Raman signal intensity and molecule concentration, which allows for compound quantification after signal calibration.[5] Raman spectroscopy can be applied in-line, on-line, or at-line for the automated monitoring of bioreactor processes, using immersion probes, flow-cells, or measurements through glass windows.[6,7] When applying in-line Raman spectroscopy in cell cultures through immersion probes, the obtained spectra contain contributions from all compounds in the medium. This allows for multiplexed monitoring with a single probe, but this also makes the signal highly complex. To address this complexity, multivariate modeling approaches based on dimensionality reduction and linear regression are commonly used to extract relevant spectral features for a target molecule. These models are typically calibrated with a dataset of Raman spectra capturing variations in the process, combined with quantitative reference measurements of the compound of interest. A calibrated model translates new spectral data into quantitative predictions for the compound of interest by applying learned weights to the spectral features associated with the compound. Through this approach, a single signal can be processed by multiple models to quantify various compounds simultaneously. Reported studies show that similar spectral data pre-processing strategies are often used to establish models for different compounds.[8]

The aim of data pre-processing is to correct for signal distortion to ensure that model calibration and prediction is based solely on the variations linearly correlated with the concentration of the molecular compounds of interest.[9] However, data pre-processing steps should be applied with caution as excessive adjustments may introduce undesired spectral artifacts. It is therefore essential to have a good understanding of the multiple sources of signal distortion during bioreactor processes. Spectral distortion in Raman spectra can occur in three categories: baseline shifts, peak shifts over the wavenumber axis, and peak intensity changes not related to concentration changes. All these types of distortion can potentially decrease quantitative model performance by disrupting signal linearity and the alignment of model weights to the appropriate wavenumber variables. Raman spectra acquired in-line in bioreactor systems are subject to multiple sources of signal distortion and noise that can affect the spectra negatively. Strong background fluorescence from compounds in the sample can potentially mask signal of interest, making it challenging to detect and analyze subtle spectral changes.[10] In addition, particles such as cells, cell debris, and bubbles with sizes near the excitation laser wavelength can induce undesired optical scattering effects, leading to Raman signal attenuation or distortion.[11] These effects become more pronounced as a cell culture progresses, as increasing biomass concentration and the accumulation of fluorescent compounds further amplifying scattering and fluorescence effects.[12–14] Whereas molecules and particles significantly smaller than the excitation wavelength ($\pi d/\lambda \ll 1$) scatter light isotropically according to Rayleigh scattering, larger particles ($\pi d/\lambda \sim 1$, $\pi d/\lambda \gg 1$) can scatter light asymmetrically, and predominantly in the forward direction.[11] The increased forward scattering and multiple scattering events by particles can lead to a reduction in the measured signal by in-line probes that use backscattering as measurement mode. While the heterogeneous composition of yeast biomass should give rise to spectral bands associated with proteins, lipids, and nucleic acids,[15] in-line Raman spectra of yeast suspension cultures are often dominated by non-linear spectral extinction.[16] The yeast *Saccharomyces cerevisiae* has an average single cell diameter of 8 μm,[17] significantly larger than the laser excitation wavelengths used by the Raman spectroscope (typically in between 532 nm and 1064 nm). This means that the cells can attenuate spectral features of other process compounds by causing anisotropic light scattering. The dominance of the resulting extinction effect complicates quantitative modeling approaches, and the spectral fingerprint related to the yeast cell's molecular composition has not yet been observed during in-line measurements. To remove extinction effects caused by biomass to ensure high quantification model performance for other molecular compounds in the bioreactor, stable peaks from medium sulfate and water have been used as internal normalization standards. This approach is based on the assumption that sulfate or water have a constant concentration and that the presence of biomass leads to a uniform signal extinction over the spectral fingerprint region.[18,19] In other cases, fluorescence and scattering effects are corrected using spectral normalization steps in combination with Whittaker baseline corrections that fit a smooth baseline using penalized least squares, followed by baseline subtraction.[4,20] Within bioreactor processes, optical scattering effects are not limited to cells, as bubbles formed in the bioreactor can reach sizes at which anisotropic light scattering occurs.[21] It is essential to understand spectral attenuation caused by bubbles as recent efforts in Raman spectroscopy model calibration involve miniaturization, flow-cell measurements, and high-throughput data collection. Some of these systems do not introduced bubbles in the matrix, which may lead to poor model transferability to bioreactor applications.

In addition to baseline distortions and signal extinction, changes in measurement conditions affecting molecular vibrations can cause unwanted peak shifts and intensity changes. An increase in system temperature can lead to the lengthening of molecular bonds by thermal expansion, lowering the vibrational frequency that causes spectral features to shift toward lower wavenumbers (red shift).[22]

Furthermore, an increase in temperature can decrease the population of molecules occupying the ground vibrational state, reducing the measured Stokes scattering intensity.[23] The level of hydrogen bonding in the medium can also affect vibrational frequencies, and several process parameters can dictate hydrogen bonding between water and medium compounds (e.g., temperature, ionic strength, pH). The spectral baseline caused by the cell culture medium predominantly consists of contributions from water, with features belonging to restricted translational and librational movements in the low wavenumber region (< 800 cm^{-1}), the water HOH-bending peak at 1641 cm^{-1}, and the OH-stretching modes in the high wavenumber region (> 3000 cm^{-1}).[24] The stability of this water baseline is dependent on multiple medium factors, such as the temperature,[25] presence of hydrogen bonding compounds, and salt concentration.[26] Conformational changes of these water bands can cause misalignment in spectral baselines and influence the efficiency of common data pre-processing strategies.

The position of key spectral features along the wavenumber axis must remain stable, as misalignment between the wavenumber variables and weights assigned by the model can lead to impaired predictive performance.[27] Peak shifts are especially problematic for sharp spectral features that comprise only a few wavenumbers, where a small wavenumber shift can lead to large prediction errors. Small shifts can be less problematic for broad spectral features as the prediction is based on a wider span of variables, providing more robustness against misalignments. However, when broad features overlap with the signal of other compounds, a model has to decompose the peak and correct for the overlap,[28] again increasing the sensitivity to wavenumber shifts. Misalignment can also affect model performance through data pre-processing. For example, internal standard normalizations can be sensitive to wavenumber shifts due to the high dependency on a singular spectral feature, where a misalignment will lead to a skewed correction of the entire spectra. Derivative-based pre-processing steps amplify a spectrum's inflection points, causing sharp minima and maxima in the derivative spectrum, and peak shifts were reported to increase prediction errors.[29] The importance of minimizing the impact of spectral misalignment is reflected by the availability of peak alignment methods correcting wavenumber shifts caused by changes in measurement conditions or differences between analytical instruments.[30]

We need to understand how spectra are influenced by measurement conditions to build robust and accurate prediction models for inline Raman spectroscopy. In this work, we systematically explore the individual influence of temperature, bubble quantities, viscosity, and *S. cerevisiae* biomass on Raman spectra. The resulting spectra are analyzed for baseline shifts, wavenumber shifts, and changing peak intensities to determine the spectral contributions of each parameter as well as the potential impact on data pre-processing strategies and quantitative model performance. These findings contribute to the understanding of spectral distortion in bioreactor-based cell cultures. This knowledge will support the development of more robust and accurate quantification models, and facilitate the use of spectral data obtained from different experimental setups and processes. Moreover, improving knowledge on the spectral contribution of yeast biomass provides the means to critically evaluate standard quantitative modeling approaches and the development of innovative biomass quantification methods.

2 | MATERIALS AND METHODS

2.1 | Measurement setup

2.1.1 | Bioreactor and controller setup

All experiments were performed in an Applikon Bio 2 L bioreactor system (Getinge, Sweden). To prevent light contamination in the Raman measurements, the bioreactor was encapsulated with a custom PVC light cover. The temperature was controlled by a Biostat B-Plus controller (Sartorius Stedim, Germany) while the stirring speed was controlled by an Applikon ADI 1032 Stirrer Controller P100 (Getinge, Sweden).

2.1.2 | Raman signal acquisition

A Raman RXN2 analyzer (Endress + Hauser Inc., Switzerland) equipped with a 400 mW 785 nm laser was connected to the bioreactor via an RXN-10 optical fiber and bIO-Optic immersion probe. The immersion probe was mounted through the bioreactor head plate and submerged into the liquid, and sterilized by autoclaving along with the bioreactor when necessary. Spectra were collected over the range of 100–3400 cm^{-1} with a resolution of 4 cm^{-1}, and a 60-s acquisition time resulted in detector saturations between 30% and 58%. The Raman spectroscope was set to continuously collect 60-s spectra, and at least 10 spectra were acquired per measurement condition. This resulted in low noise measurements.

2.2 | Bioreactor parameter experiments

2.2.1 | Media solutions

Four different types of media were used to study the bioreactor parameter effects: (1) Distilled water, (2) Synthetic media, (3) Synthetic media with low glucose concentration ($c_{glucose}$ = 24.4 g/L), (4) Synthetic media with high glucose concentration ($c_{glucose}$ = 47.6 g/L). The synthetic media were prepared with distilled water and contained 5 g/L $(NH_4)_2SO_4$ (Merck, Darmstadt, Germany), 3 g/L KH_2PO_4 (Merck, Darmstadt, Germany), and 0.5 g/L $MgSO_4 \cdot 7H_2O$ (Honeywell, Seelze, Germany).[31] The media were adjusted to pH 6.0 with 2 M KOH (Merck Sigma, Darmstadt, Germany), and 50% w/v glucose solution was prepared with glucose monohydrate (Merck, Darmstadt, Germany) and added to the desired concentration. The synthetic medium was completed with 0.2 g/L Antifoam-C (BASF, Ludwigshafen, Germany). An additional 15% vol/vol glycerol (Merck Sigma,

Darmstadt, Germany) solution was prepared for studying the effect of viscosity on the spectra.

2.2.2 | Temperature control

Temperature effects on the Raman spectra were studied in the range of 20–40°C with step sizes of 5°C. The temperature values were reached using the bioreactor thermostat and controlled with the Biostat B-plus bioreactor controller. Media mixing was performed by continuously stirring at 830 rpm without sparging. A maximum deviation of 0.1°C from the setpoint was allowed during the measurements.

2.2.3 | Sparging and bubble size control

The bioreactor stirrer was operated at 80, 500, 675, and 830 rpm to form different quantity of bubbles and bubble sizes without the need of sparging. Bubble formation started at 500 rpm, and increased for higher stirring speeds (Figure S2). During these measurements the temperature was kept constant at 30°C using the same setup as described in Section 2.2.2.

2.2.4 | Viscosity control

The 15% v/v glycerol solution was used in combination with active temperature control to generate different viscosity levels in the bioreactor. The temperature of the glycerol solution was operated in the range of 20–45°C with a step size of 5°C. A Lovis 2000 M/ME viscometer (Anton Paar, Austria) was used to measure the viscosity of this solution at each temperature. During measurements, the bioreactor was mixed by stirring at 830 rpm without sparging. The viscosity reference measurements are provided in Table S1.

2.3 | Fermentations and biomass measurements

2.3.1 | Batch fermentation

Two batch fermentations were conducted with an inoculation cell density of 0.015 g/L. The yeast strain *S. cerevisiae* CEN.PK113-7D was used for all cell culture experiments.[32] All cultures were grown on sterile synthetic media (see Section 2.2.1) supplemented with 0.2 g/L sterile Antifoam-C (BASF, Ludwigshafen, Germany) and filter sterilized vitamin solution (in-house) after autoclaving. Glucose was used as a carbon source, and an initial concentration of 40 g/L was reached by the addition of sterilized 50% glucose solution (see Section 2.2.1). Medium aeration was performed by stirring at 830 rpm and sparging air at 0.5 L/min. A pH of 6.0 was maintained by the addition of 2 M KOH, and the temperature was kept constant at 30°C. The working volume of the reactors was 1 L, and the fermentations were operated until glucose depletion was detected by the drop in off-gas CO_2 measured with a ServoPRO 4900 off-gas analyzer (Servomex, UK).

2.3.2 | Reference sampling

Samples of the supernatants of the batches were analyzed for their ethanol and glucose concentrations using an Agilent 1260 Infinity HPLC (Agilent Technologies, USA). A BIO-RAD Aminex HPX-87H (300 × 7.8 mm) cation-exchange column (Bio-Rad, USA) operated at 60°C was used with a 0.5 g/L H_2SO_4 eluent at a flow rate of 0.6 mL/min. The injection volume was 5 µm, and an Agilent 1260 refractive-index and variable wavelength detector were used for sample characterization.

The cell density of the fermentations was determined off-line by optical density at a wavelength of 660 nm (OD660) using a Libra S11 spectrophotometer (Biochrom, UK). The dry biomass weight was measured by loading 10 mL of cell suspension on nitrocellulose membrane filters (pore size, 0.45 µm; Gelman Laboratory, USA), drying the filters in a microwave, and subsequently weighing the dry biomass on a precision scale (Mettler Toledo, USA).

2.3.3 | Biomass harvest and measurement

After glucose depletion occurred in the batch fermentations, the bioreactor broth was harvested and the biomass was washed twice by centrifuging and resuspending the cells. The suspension was centrifuged at 5000 rpm for 5 min in 400 mL bottles using an Avanti J-E centrifuge (Beckman Coulter, USA) to pellet the cells. After discarding the supernatant, the cell pellet was resuspended in fresh synthetic media. After the second washing step, the biomass was resuspended in 350 mL of synthetic media to a final concentration of 15 g/L. The washed cell suspension was added in steps of 25 mL to a bioreactor with 700 mL of clean synthetic media to measure concentration ranges of biomass. The Raman measurements were performed while maintaining 830 rpm of stirring, sparging with 0.5 L/min of air, and temperature control at 30°C. During the measurements, samples were taken to determine the cell viability using a NucleoCounter NC-202 (Chemometec, Denmark).

2.4 | Data analysis

2.4.1 | Spectral processing

Spectral pre-processing was performed in PLS_Toolbox (v 9.3, Eigenvector Research, WA) running on MATLAB 2023a (MathWorks, WA), and Python 3.10 using libraries from scikit-learn (https://scikit-learn.org[33]) and Chemotools (https://paucablop.github.io/chemotools/[34]). For each measurement condition, 10 spectra of 1 min were averaged to a single spectrum by an in-house Python script to improve spectral quality and reduce noise.

2.4.2 | Peak shift detection

Peak shift quantification was performed by determining the exact peak location. The location of spectral peaks was determined using the zero-crossing point after spectral derivatization, which coincides with the position of a peak. Peak position determination was performed using an in-house Python script, and the workflow consisted of three steps. First, spectra of the bioreactor parameters and biomass measurements were reduced to the fingerprint region (350–1800 cm^{-1}) to minimize the leverage of the high spectral tails on the baseline correction. Second, AirPls baseline correction ($\lambda = 300$) was applied to remove spectral baselines, thereby reducing the influence of baselines on peak locations. Third, a second-order derivative (15-point window, second order polynomial) was taken from the baseline-corrected spectra. Fourth, linear regression was applied between the datapoints before and after the zero-crossing of the second derivative spectra, and the exact crossing point was calculated to determine the peak position.

2.4.3 | Signal extinction analysis

The decrease in peak intensity was measured to determine the level of signal extinction caused by bioreactor parameters and biomass. The spectra were reduced to the fingerprint region (350–1800 cm^{-1}) and pre-processed using the AirPls baseline correction ($\lambda = 300$), effectively removing the baseline while retaining the peak intensity in relation to the original baseline, as well as the relative differences between the individual measurements. After pre-processing, the absolute peak intensity was used for analysis.

3 | RESULTS AND DISCUSSION

Spectral distortion as a result of the bioreactor process parameters temperature, bubble quantity, and viscosity, as well as biomass concentration, was investigated. The influence on the spectral baseline was determined by inspecting the full Raman spectrum, and changes in wavenumber shifts and peak intensities were quantitatively assessed using four pre-defined peaks: immersion probe window (406 cm^{-1}), water HOH-bending (1641 cm^{-1}),[25] and when present in the mixture, the peaks of media sulphate (981 cm^{-1}) and glucose COH-bending (1125 cm^{-1}).[35] Four measurement matrices with known spectral features were used to perform these experiments: (1) distilled water, (2) synthetic media, (3) synthetic media with low glucose concentration (25 g/L), and (4) synthetic media with high glucose concentration (50 g/L). To study the effects of viscosity, a mixture of 15% (v/v) glycerol solution in water was measured under different temperatures to change the liquid viscosity without adjusting the absolute glycerol concentration.

3.1 | Spectral effects of temperature

Changes in temperature can occur during process development or when spectral data is combined from different (miniaturized) experimental setups. Temperature influences the vibrational state populations of molecules and alters hydrogen bonding dynamics, both between water molecules and between water and other compounds in the medium. These changes can alter peak positions and intensities in a Raman spectrum. The spectral baseline of cell culture media is primarily influenced by contributions from water, and the resulting spectral changes in the water matrix due to temperature increases from 20 to 40°C are shown in Figure 1. The baseline effects of temperature on the other matrices are shown in Figure S1.

The largest spectral baseline changes occurred in the broad bands related to the vibrational modes of water in the low (< 800 cm^{-1}) and high (> 3000 cm^{-1}) wavenumber regions. The baseline below 200 cm^{-1} (Figure 1a) showed an increase in intensity at higher temperatures as a result of the increasing band at 60 cm^{-1} just outside of the spectroscopes range (<100 cm^{-1}), which belongs to restricted translational movements of water molecules.[36,37] Furthermore, the baseline from approximately 300 to 800 cm^{-1} also increases with higher temperatures as the underlying broad features associated with the librational modes of water become more prominent due to the reduced hydrogen bonding and increased molecular motion.[24] The observed baseline changes in the low wavenumber region were similar in the synthetic media matrices (Figure S1). The bands in the high wavenumber region (Figure 1b) originate from OH-stretching vibrations of water, and although a large section of these peaks is outside of this spectroscope's measurement range (>3425 cm^{-1}), some of the conformational changes are still visible between 3000 and 3425 cm^{-1}. For example, higher temperatures weaken hydrogen bonds between water molecules, reducing the formation of large water molecule clusters, which typically decreases the intensity of the strong hydrogen bonding band at 3200 cm^{-1} and increases or broadens the intensity of the weaker hydrogen bonding band around 3400–3600 cm^{-1}.[24,38] For all four matrixes, a decrease in the band at 3200 cm^{-1} was observed (Figure S1), while the visible part of the band at 3400 cm^{-1} increased in water and decreased in the synthetic media matrices. This difference is most likely caused by the dissolved salts in the synthetic medium, which can disrupt the hydrogen bonding behavior of water molecules.[39] The conformational change between these two OH-stretching bands in water matches examples in the field of Raman thermometry, where the ratio between these bands is used as an indicator for system temperature.[40] However, as the majority of this second band was outside of the detectable range for this spectroscope, further analysis was not performed on this region.

Four peaks were quantitatively analyzed for wavenumber shifts caused by temperature, and the results are displayed in Figure 2. An average peak shift across the four different mixtures of 0.73, 0.61, and 0.80 cm^{-1} was found for the immersion probe glass, sulphate, and glucose peaks, respectively, while the water HOH-bending peak

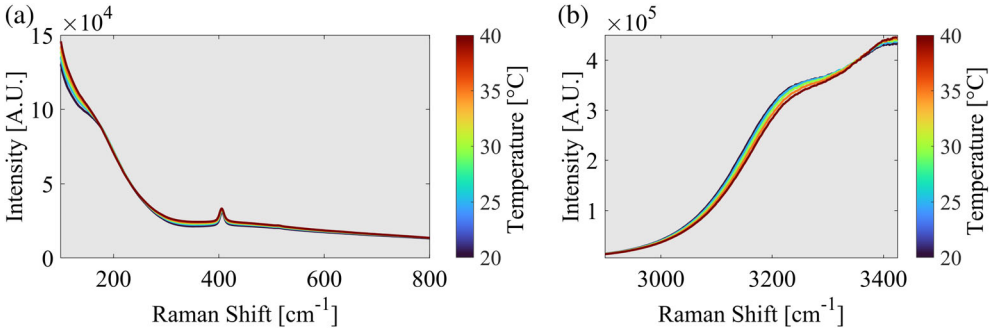

FIGURE 1 The low (a) and high (b) wavenumber region of water matrix for a temperature range from 20 to 40°C (blue to red in the color bar). The displayed spectra are the average of 10 individual 60-s spectra acquired at each temperature.

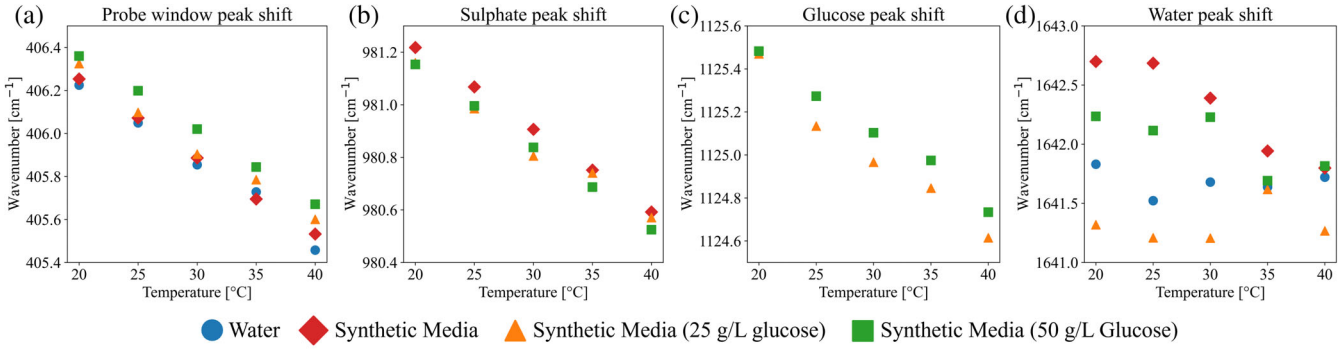

(e)

Measurement Matrix	Peak intensity decrease over temperature range			
	Probe window	Sulphate	Glucose	Water
Water	1.89%			5.38%
Synthetic Media	2.61%	6.57%		1.28%
Synthetic Media (25 g/L glucose)	2.54%	4.57%	7.07%	1.53%
Synthetic Media (50 g/L glucose)	2.29%	2.23%	2.23%	2.03%
Average	2.33%	4.46%	4.65%	2.56%

FIGURE 2 The effect of temperature on the peak locations of probe window (a), media sulphate (b), glucose (c), water HOH-bending (d), and the total intensity decrease per peak and measurement matrix (e). The peak location was derived by pre-processing the spectra with AirPls baseline correction (lambda = 300), taking a Savitzky Golay derivative (first order, 15-point window length), and interpolating the zero-crossing point of the x-axis.

at approximately 1641 cm^{-1} showed a less consistent shift pattern. A peak shift to lower wavenumbers can occur due to thermal expansion at higher temperatures, causing increasing bond lengths and the disruption of hydrogen bonds. Both of these factors can reduce the energy difference between the ground and elevated vibrational states, thereby affecting the peak position. In AirPls baseline corrected spectra, the temperature increase led to an average relative intensity decrease of 2.33%, 4.46%, 4.65%, and 2.56% for the probe window, sulphate, glucose, and water peaks across all measurement matrixes (Figure 2e).

Figure 2a shows that the linear trajectory of the probe window peak shifts at 406 cm^{-1} is similar for each matrix, where the mean peak shift per 5°C step was 0.18 cm^{-1} with a standard deviation of 0.03 cm^{-1} across all measurement matrixes. Peak shifts when measuring crystal structures are commonly studied over wider temperature ranges, and the observations on the probe window glass match in order of magnitude with examples of Raman sapphire crystal studies in literature (~0.41 cm^{-1} per 20°C).[41] For the two matrices containing glucose it was observed that the probe window peak is identified at slightly higher wavenumbers compared to the matrices without glucose. Glucose has a broad CCC-bending peak at 432 cm^{-1}[35] that partly overlaps with the 406 cm^{-1} probe window peak, thereby slightly affecting the peak position in the 25 and 50 g/L glucose synthetic media samples. The average peak shift for sulphate (0.61 cm^{-1} at 981 cm^{-1}) is comparable to observations under similar conditions in literature (~0.30–0.70 cm^{-1}), where it was also found to be dependent on the salt concentration.[42,43] The average glucose peak shift (0.80 cm^{-1} at 1125 cm^{-1}) could not be directly verified with existing literature under similar measurement conditions. The changing peak positions of sulphate and glucose can be the result of changes in hydrogen bonding, while for sulphate, ionization effects in the media can also play a role when temperature changes. The water peak at approximately 1641 cm^{-1} shown in Figure 2d belongs to the HOH-bending vibrational mode. The HOH-bending is more confined to individual water molecules and it should therefore be less affected by hydrogen bonding.[25] The results do not show a consistent pattern in the wavenumber shift and the detected decreases in peak intensities were relatively small (2.56% on average). A possible explanation for

the decrease in measured peak intensities relative to the baseline is the increase of molecules in higher vibrational states when temperature increases. As the Raman spectroscope used in this work measures Stokes scattering, which primarily occurs when molecules are in the ground vibrational state, a shift of molecules to higher vibrational states could decrease the measured signal intensity.

The experimental data showed baseline and conformational changes mainly in the low and high wavenumber regions as a result of temperature changes. For the application of Raman spectra for quantitative real-time monitoring, spectra are typically reduced to the fingerprint region (around 350–1800 cm^{-1}) as a part of data preprocessing, sometimes including the region in between 2800 and 3000 cm^{-1}, as the excluded regions contain little chemical information on biological molecules. Therefore, the expectation is that temperature-induced changes observed at the tails of the spectra (<300 cm^{-1} and >3000 cm^{-1}) will not influence model building unless the full spectra are used for analysis. Thus, if the full spectrum is subjected to pre-processing involving polynomial fitting, the intensity differences in the spectral tails can strongly influence baseline and scatter corrections by exerting high leverage on the polynomial fit. As a consequence, improper baseline alignment may occur in key spectral areas such as the fingerprint region and thereby impact the accuracy of compound quantification using chemometric models.

The observed peak shifts and intensity changes as a result of changing temperature pose a far larger challenge for model building, as these phenomena can directly affect the linear correlation between signal intensity and molecule concentration and can lead to spectral misalignments between peaks and model coefficients. In general, there are few bioreactor or cell culture processes that see a temperature shift of more than 5°C (leading to an average shift of 0.2 cm^{-1} in the glucose peak). However, peak shifts can be problematic in model calibration approaches where data from different experimental sources with varying levels of temperature control are combined (e.g., bioreactor, glassware, flow-cells, and alternative miniaturized setups) or during process development. Calibrating a model with samples at room temperature and subsequently applying it to cell culture conditions may lead to poor predictive performance as a result of spectral feature misalignment and peak intensity differences. A potential mitigation strategy is the use of spectral alignment techniques to correct feature positions between different measurement conditions.[30] In applications where multiple spectrometers are used across different facilities, these methods are already implemented to correct for variations between instruments.[44] Peak alignment approaches, combined with methods to account for normalizing the changes in peak intensities, could effectively standardize the spectra and facilitate the fusion of data obtained from various sources and at different process conditions.

3.2 | Spectral effects of bubbles

Both bubbles and cells attenuate Raman spectra by acting as light scattering particles.[16,21] To isolate the spectral contribution of biomass that can be used as input for biomass quantification models, it is key to understand the light-attenuating effects of bubbles. To this end, bioreactors were operated at different impeller speeds (80, 500, 675, and 830 rpm) to generate bubbles of different sizes and quantities within the four matrices. We observed bubble formation around the baffles starting at 500 rpm, which was therefore chosen as the second step after the 80 rpm baseline condition. Bubble formation increased with higher rpms regardless of the mixture composition (Figure S2). This section focuses on peak intensity changes to assess the impact of bubbles, as a peak shift analysis did not result in peak shifts larger than 0.11 cm^{-1} across different impeller speeds (Figure S3). Although the water HOH-bending peak showed peak shifts of up to 0.67 cm^{-1}, the inconsistent patterns were attributed to noise and therefore considered to be independent of the bubbles. Figure 3 shows the impact of bubble formation on the absolute peak intensity for the probe window, sulphate, water HOH-bending, and glucose peak. The intensity decreases per peak and measurement matrix for increasing stirring rates are summarized in Figure 3e.

Interestingly, extinction of 0.87% to 4.68% for the peak of the immersion probe (406 cm^{-1}) was observed when measuring the synthetic media matrices. This peak should not be affected by bubbles behind the window, as seen for water and synthetic media without glucose, because it arises from the immersion probe itself. For the synthetic media matrices with glucose, this observed intensity change might be due to extinction of the broad glucose CCC-bending peak at 432 cm^{-1} by the bubbles, which partly overlaps with the probe window peak at 406 cm^{-1},[35] similar to the results in the temperature change experiment. The extinction of the sulphate, glucose, and water peaks was 6–8% in the synthetic media measurements, while the concentration of these compounds remained constant. For the water matrix, the probe window and water HOH-bending peaks only showed a 0.42% and 1.30% decrease in peak intensity, respectively. This aligns with the visual inspection of the overall spectral changes in water, which are small compared to those in synthetic media (Figure S4). The synthetic media matrices contained high salt concentrations and antifoam-C that can impact the bubble formation while stirring. High salt concentrations increase surface tension and can reduce bubble coalescence, thereby increasing the stability of small bubbles when compared to water.[45] Antifoam-C works as a defoaming agent by lowering surface tension and is added to cell culture medium to displace bubble stabilizing surfactants. Despite the presence of antifoam, it was visually observed that bubble formation increased drastically in the synthetic media matrices when compared to water, leading to a higher bubble density during the Raman measurements and thus greater signal attenuation. The bubble size and quantity were not measured during these experiments, and there is only visual proof of the increasing bubble quantity and decreasing bubble size (Figure S2). The exact bubble and particle size distribution during bioreactor processes is challenging to estimate and measure, and is an active field of research.[46]

The reported measurements here show that the spectral extinction caused by increasing bubble quantities and decreasing bubble size is significant (up to 8%), especially considering the constant

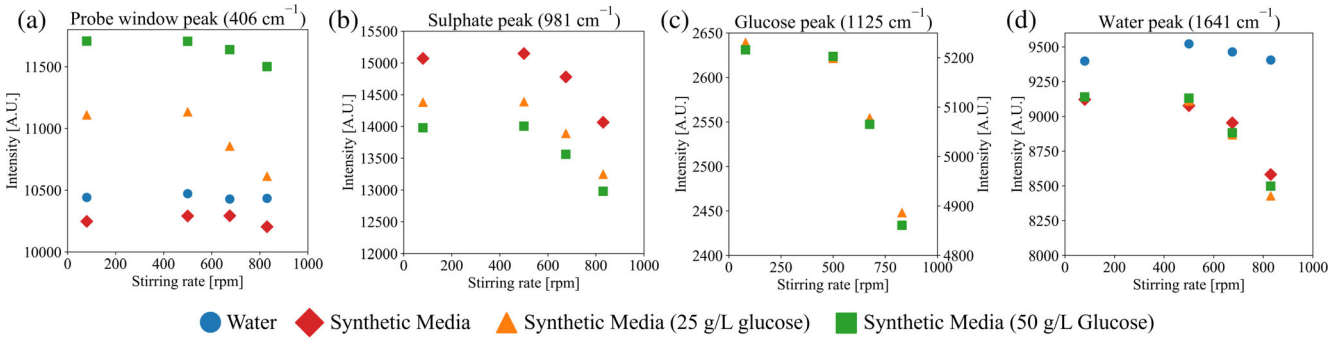

(e)

Measurement Matrix	Intensity decrease over RPM range			
	Probe window 406 cm^{-1}	Sulphate 981 cm^{-1}	Glucose 1125 cm^{-1}	Water 1641 cm^{-1}
Water	0.42%			1.30%
Synthetic Media	0.87%	7.14%		5.91%
Synthetic Media (25 g/L glucose)	4.68%	7.93%	7.25%	7.81%
Synthetic Media (50 g/L glucose)	1.77%	7.31%	7.31%	7.02%

FIGURE 3 The effect of bubble quantity caused by increasing stirring speeds on the peak intensities for the probe window (a), media sulphate (b), glucose with low concentration on the left y-axis and high concentration on the right y-axis (c), water HOH bending (d), and the total intensity decrease per peak and measurement matrix due to bubble quantity increase (e). The datapoints were acquired by taking the absolute peak intensities at the indicated wavenumbers after pre-processing spectra with AirPls baseline correction (lambda = 300).

concentration of compounds in the samples during the measurements. This means that the observed peak extinction can disrupt the proportionality between signal intensity and molecule concentration, and that bubble size and quantity should be taken into account as signal-attenuating particles during model development. Furthermore, the production of fermentation compounds, such as ethanol, glycerol, or extracellular proteins, can also affect the surface tension and thereby bubble coalescence.[45] The combination of these changing factors over the course of a fermentation makes bubble formation a dynamic factor during a single process. In terms of high-throughput model calibration for quantitative monitoring, differences in signal intensity between spectra obtained in bioreactor settings and (miniaturized) high-throughput setups may arise due to the absence of bubbles (e.g., as seen for flow-cells and sample chambers). For example, the sulphate peak that is often used as a normalization reference[18] seems to suffer from similar levels of signal extinction compared to the glucose and water peak. As the peak shift was minimal for these spectra and the signal extinction appears uniformly distributed over the fingerprint peaks, sulphate normalization would lead to appropriate correction of signal extinction caused by bubbles. In cases where the extinction is not uniformly distributed, multiplicative scatter corrections such as extended multiplicative scatter correction (EMSC) would be more appropriate. In both cases, the normalization step should be critically evaluated to ensure that spectra from different experimental setups are adjusted equally to make signal intensities representative of the environment in which the models will be applied.

3.3 | Effects of viscosity

Cell culture media viscosity is influenced by changing concentrations of substrates and products, which interact with water through

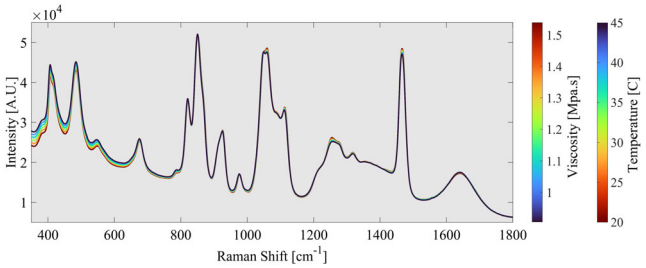

FIGURE 4 The Raman spectra fingerprint region of 15% v/v glycerol solution measured at a viscosity ranging from 1.55 to 1.03 mPa.s (second colorbar) obtained by increasing the temperature from 20 to 45°C in increments of 5°C (first colorbar). The displayed spectra are the average of 10 individual 60-s spectra acquired at each temperature step.

hydrogen bonding, as well as the accumulation of biomass that increases the viscoelastic properties of the medium. To study the spectral changes caused by viscosity, a 15% v/v glycerol solution was measured under temperatures ranging from 20 to 45°C with increments of 5°C. Increasing the temperature leads to the dissociation of hydrogen bonds between glycerol and water, and allowed a viscosity range of 1.55 to 1.03 mPa.s, thereby simulating a yeast fermentation of up to 55 g/L of yeast biomass[47] (the measured viscosities are shown in Table S1). This approach was selected to allow for viscosity adjustments without changing the compound (glycerol) concentrations. Several peaks belonging to glycerol vibrational modes were investigated for wavenumber shifts and intensity changes. The fingerprint regions of the acquired spectra are shown in Figure 4 (peak shifts are shown in Figure S5).

As a changing temperature setpoint was required to control the viscosity of the 15% v/v glycerol solution, the data does not allow

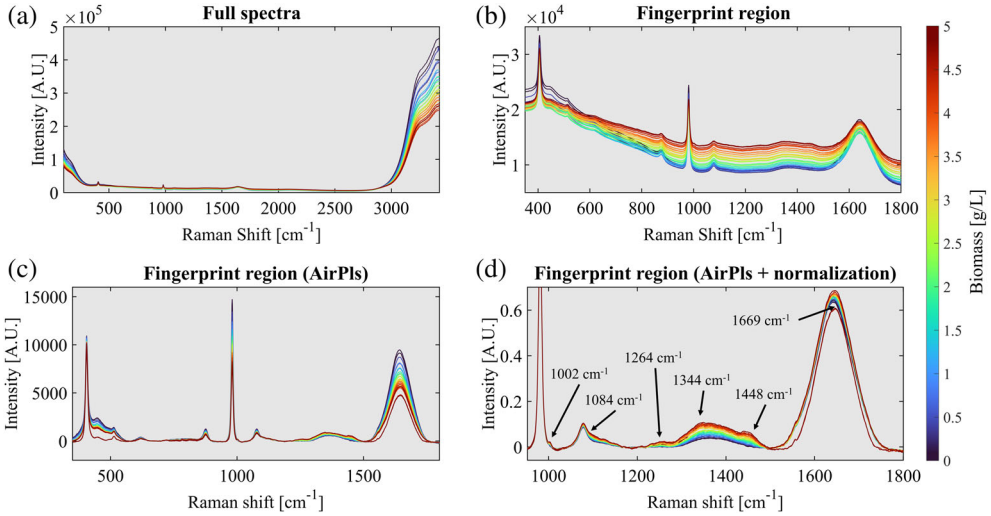

FIGURE 5 The full (a), fingerprint region (b), AirPls (lambda = 300) pre-processed fingerprint region (c), and AirPls (lambda = 300) followed by sulphate peak normalization pre-processed fingerprint region (d) of spectra acquired for 0 to 5 g/L isolated biomass (blue to red in the colorbar). Each displayed spectra is the average of 10 individual 60-s spectra acquired at a single concentration step.

evaluation of the effects of temperature and viscosity independently. In the previous temperature measurements (Section 3.1) an increasing temperature generally led to an increasing baseline intensity in the low wavenumber range (<800 cm^{-1}) and peak shifts toward lower wavenumbers (up to 0.8 cm^{-1}). Similar spectral changes were observed in the 15% v/v glycerol mixture, where the baseline in the low wavenumber region shifted up and the glycerol peaks shifted to lower wavenumbers. Glycerol fingerprint features, such as the two CC-stretch (821 and 851 cm^{-1}) and two CH_2-rock (925 and 977 cm^{-2}) peaks,[48] moved to lower wavenumbers by 0.63, 0.95, 0.83, and 0.84 cm^{-1}, respectively. These peak shifts were comparable in magnitude to the shifts observed for other peaks analyzed during the temperature experiments. The overlap of glycerol peaks in the 1000 to 1350 cm^{-1} region complicates peak position determination due to influences of shouldering peaks. The peak shift determination method calculated a shift to lower wavenumbers by 2.48 cm^{-1} for the observed spectral features at 1050 and 1060 cm^{-1} (Figure S5). Additionally, a 1.50 cm^{-1} shift was calculated for the peak at 1111 cm^{-1} attributed to the CO-stretch vibrational mode involved in hydrogen bonding. However, the large overlap with the shoulder at 1090 cm^{-1} coming from a CH_2 rocking mode affects the accuracy of peak shift determination. The overall observed effects (hydrogen bond strength) match those seen during the changing temperature experiments, and no additional effects of viscosity could be identified. It should be noted that viscosity is influenced by multiple factors beyond hydrogen bonding during fermentation, such as ionic strength and cell density, where various chemical and physical properties of the medium may affect Raman spectral features differently.

3.4 | Effects of yeast biomass

Yeast cells constitute the majority of the particulate matter during fermentation in a bioreactor. The *S. cerevisiae* cells used in this work have an average diameter of ~8 μm in their single cell form with an ellipsoidal shape,[17] and at this size the cells can cause anisotropic light scattering ($\pi d/\lambda \gg 1$) when considering the excitation laser wavelength of 785 nm. To determine the impact of anisotropic light scattering, two batch fermentations were operated to generate yeast cells for the measurement of isolated biomass, using a concentration range 0 to 5 g/L. The yeast cell viability was above 96% during all the washing steps and measurements, minimizing the contribution of different scattering effects and fluorescence as a result of dead cells and cell debris. The experiment was performed twice with biomass from two individual batch cultures to test for reproducibility (Figure S6) and all resulting spectra of the isolated biomass are shown in Figure 5. Two high concentration biomass spectra were poorly corrected by the baseline correction (Figure 5c) and therefore removed for further analysis.

Peak shift analysis resulted in an average wavenumber shift of 0.36, 0.29, and 1.90 cm^{-1} for the probe window, sulphate, and water HOH-bending peaks, respectively (Figure S7). Increasing the biomass concentration was not expected to affect vibrational modes and cause peak shifts, and this is most likely due to the addition of underlying spectral features. The overall spectral changes caused by biomass did not directly show distinct peaks or spectral markers, as is typically observed for molecular compounds. The major observed spectral effects over the full spectral range were a strong intensity decrease in the low (<800 cm^{-1}) and high (>3000 cm^{-1}) wavenumber regions (Figure 5a), and a slight baseline increase caused by background fluorescence in the fingerprint region (350–1800 cm^{-1}, Figure 5b). After correcting for this fluorescence baseline increase in the fingerprint region with an AirPls baseline correction, the impact of increasing biomass becomes visible. Figure 5c shows the extinction of other spectral features (sulphate peak 981 cm^{-1}, water peak 1641 cm^{-1}) relative to the baseline for increasing biomass concentration. Subsequent normalization to correct for the signal extinction using the sulphate peak[4] reveals an increase in intensity in the 1000–1500 cm^{-1} range for increasing biomass (Figure 5d). The intensity changes in this range linearly correlate with the biomass concentration (Figure S8) and can be associated with the composition of *S. cerevisiae*, which is mainly characterized by a heterogeneous distribution of protein and lipid

structures.[49] These compounds typically display broad bands, where lipids and proteins have strong features in the 1400–1500 cm^{-1} range,[50] while proteins also display broad features in the 1200–1400 cm^{-1} range.[51] Moreover, the observed signal in these regions aligns with Raman microscopy measurements of *S. cerevisiae* strains in literature on strain discrimination.[15] The spectral features indicated in Figure 5d could be linked to phenylalanine (1002 cm^{-1}),[52] phospholipids (1084 cm^{-1}),[53] broad amide III bands (1246 cm^{-1}),[51] protein CH deformation (1344 cm^{-1}), CH_2-deformation of proteins and lipids (1448 cm^{-1}), and amide I stretching (1669 cm^{-1}),[51] although the low intensity of these features makes a more exact identification of each band challenging. Nevertheless, these measurements indicate that the molecular composition of *S. cerevisiae* can be measured using in-line Raman spectroscopy, even though literature suggests that no identifiable Raman spectroscopy features are detectable with in-line measurements.[16,54] This is most likely due to the difference in pre-processing strategy, where we correct for the otherwise dominant extinction effects. The measured shift of the water HOH-bending peak to higher wavenumbers by 1.90 cm^{-1} seems to be caused by the increase of the underlying spectral feature at 1669 cm^{-1} (amide I stretching). Similarly, the increase of the spectral feature at 1002 cm^{-1} (phenylalanine) most likely caused the shift to higher wavenumbers of the sulphate peak.

The intensity of the specific peaks associated with the composition of *S. cerevisiae* is considerably lower compared to the extinction effects induced by the cells as particles. To determine the degree of signal extinction caused by the yeast cells as particles, the peak intensity of the probe window (406 cm^{-1}), sulphate (981 cm^{-1}), and water HOH-bending (1641 cm^{-1}) was determined from the AirPls corrected biomass spectra. To investigate if these peak extinctions translate to real fermentation data, a comparison was made to spectra acquired during yeast batch cultivations. Raman spectra from four individual batch cultivations with biomass concentrations reaching from 0.1 to 3 g/L were pre-processed by the same AirPls baseline correction, and the measured signal decreases are shown in Figure 6.

The pattern of signal extinction for all peaks was similar between the two isolated biomass experiments and resulted only in a slight intensity offset. The average intensity decrease of the probe window peak at 406 cm^{-1} (Figure 6a) was 4.8% and 16.1% for the isolated yeast measurements and batch fermentations, respectively, and a large offset in signal intensity between the isolated yeast measurements and batch data was observed. The difference in intensity decrease stems from a different fit of the AirPls baseline correction caused by overlapping spectral features of glucose and other compounds during the fermentations with the probe window peak. Without this overlap, it is clear that the probe window peak experiences little intensity decrease for the isolated biomass measurements compared to the fermentations. In contrast, signal extinction was comparable for the sulphate and water peaks between the isolated biomass measurements and the batch cultivations, which both show a non-linear decrease in peak intensities when the biomass concentration increases (Figure 6b,c). Increasing the yeast concentration from 0 to 5 g/L led to average signal extinctions of 44.7% and 44.6% for the sulphate (981 cm^{-1}) and water (1641 cm^{-1}) peaks, respectively. The batch cultivations only reached up to 3 g/L of biomass and resulted in an average extinction of 36.6% and 33.3% for the sulphate and water peaks. During both experiments, the sulphate and water peaks were mostly free from other overlapping molecular signals, and their concentrations are assumed to be constant, which is why these peaks are utilized as internal standards in other reported work.[4,16,18] The observed non-linear pattern for increasing the biomass concentration is similar to the observations of Yang et al. (2024) who measured the extinction of glucose and ethanol peaks.[54] Although the degree of extinction between the sulphate and water peaks appears to be similar in this work, this does not guarantee uniform extinction across the fingerprint region in the raw spectra. The AirPls baseline correction performed optimally with a lambda value of 300. Slight changes to the lambda value affected the fit of both broad and narrow peaks, which could potentially influence the measured signal extinction. Previous literature on the extinction effect of yeast cells as particles also

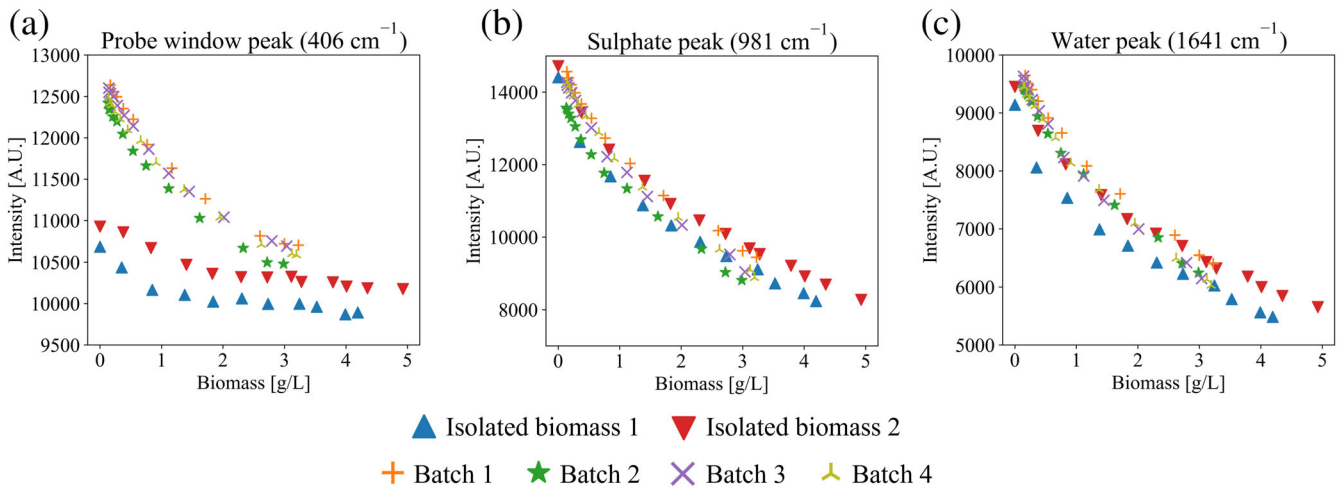

FIGURE 6 The effect of biomass on the peak intensities for the probe window (a), media sulphate (b), and water HOH-bending (c) peak. The datapoints were acquired by taking the absolute peak intensities at the indicated wavenumbers after pre-processing spectra with AirPls baseline correction (lambda = 300).

highlighted that the extinction effect is not uniformly distributed across the fingerprint region.[16,54] Therefore, the use of internal standards for normalizing extinction effects should be carefully assessed, as this does not guarantee a proper correction for features far from the internal standard.

The biomass experiment revealed weak bands associated with the molecular composition of yeast proteins and lipids in the 1000–1500 cm^{-1} region and showed a strong non-linear signal extinction for increasing concentrations. However, the detected spectral features for biomass spanned a broad range that overlaps with the strong and sharp spectral features of commonly found molecular compounds in fermentations, namely glucose and ethanol. As the increase in biomass and product concentration typically correlates strongly during fermentation, it may be unlikely for multivariate linear regression models to extract the right spectral variation for biomass from the signals of ethanol. Broad features are also more sensitive to removal by baseline and scattering corrections as these can be perceived as spectral baseline effects.

The findings in this work highlight how multivariate linear regression models can be challenged by Raman spectra from yeast cultivations, as the strong signal extinction by cells as particles disrupts the proportionality between signal intensity and molecule concentration. When looking at bioreactor applications of Raman spectroscopy over the last decades, the majority was for mammalian cell cultures such as Chinese hamster ovary (CHO) cells.[6] The typical effective pre-processing strategies for CHO cell processes include a baseline correction or derivative step followed by a standard normal variate (SNV) scatter correction,[20,55] and strong signal extinction effects as observed for yeast cells are not reported. Yeast cells are smaller and have a high optical density, which results in stronger light scattering. The extremity of signal extinction is seen even at the low yeast concentrations in this work, and this supports approaches that employ the signal extinction itself to quantify yeast biomass. For example, Yang et al. (2024) used the intensity decrease of the water HOH-bending peak to quantify biomass concentrations.[54] However, such approaches might only be viable when yeast cells are the only light scattering particles in the medium. As presented in Section 3.2, operating the bioreactor at a typical stirring rate of 830 rpm generated bubbles leading up to a 7.91% reduction of distinct peak intensity, while biomass of up to 5 g/L led to signal extinctions of 44.6%. Since the biomass can be expected to have a relatively uniform size, further research is required to determine the precise influence of bubble size and size distributions on signal attenuation. Despite the spectral distortion caused by biomass or bubbles, there have been many successful cases of monitoring compounds such as glucose, ethanol, and other products during yeast fermentation with Raman spectroscopy.[4,56] This indicates that the extinction effects can be removed from spectra with the appropriate scatter corrections and normalization steps.

4 | CONCLUSION

Raman spectroscopy is becoming an established analytical tool for cell culture monitoring and has been successfully applied to quantify small molecular compounds in real time. However, without understanding the impact of different process parameters, quantitative model performance cannot be guaranteed when leveraging data from different scales, processes, or measurement conditions. This study investigated the spectral impact of temperature, bubble quantity, viscosity, and yeast biomass. Changing the temperature in the bioreactor from 20 to 40°C resulted in a maximal peak shift of up to 0.80 cm^{-1} toward lower wavenumbers, while a decrease in peak intensity was observed of up to 4.46% (relative to the spectral baseline). An increasing number of bubbles generated through high stirring speeds resulted in signal extinction, reflected by up to 7.93% lower peak intensities in synthetic media samples. The spectral effects of liquid viscosity as a function of temperature in a 15% v/v glycerol water mixture led to complex peak shift behavior with magnitudes similar to those observed for temperature alone, and we were therefore not able to truly isolate the effects of viscosity. Increasing biomass concentrations led to strong signal extinctions of up to 44.7% in the fingerprint region, causing a significant reduction in the measured signal of peaks from compounds with constant concentrations. In addition to signal attenuation, we were able to identify weak spectral bands associated with proteins and lipids in the 1000–1500 cm^{-1} spectral region after normalizing for scattering effects. This demonstrated that spectral features related to the molecular composition of yeast cells can be detected with in-line Raman spectroscopy, although the signal extinction caused by the cells as particles remains the dominant effect.

Overall, this work shows that Raman spectra are sensitive to wavenumber shifts and peak intensity changes for different operational conditions, and that particles such as bubbles and cells can cause significant signal extinction during in-line measurements. These effects can complicate model calibration and subsequent application, as mismatches between the affected spectral features might reduce quantification accuracy. Moreover, predictive models may face difficulties in generalizing between spectra acquired from different measurement conditions, especially considering sharp spectral features spanning few wavenumbers. A better understanding of these sources of spectral noise aids in the design of appropriate data pre-processing steps, thereby removing baseline shifts, restoring linearity through normalization, and reestablishing variable alignment. Furthermore, data pre-processing and modeling strategies should be tailored to each compound of interest. For example, the spectral contribution from yeast biomass is dominated by signal extinction rather than by its molecular spectral features. The insights obtained through this work contribute to a better understanding of signal distortion in bioprocessing, thereby serving the development of robust quantification models. This work will support rapid model calibration with the use of (miniaturized) alternative setups to minimize time- and labor-intensive (re)calibration activities, thereby making real-time monitoring with Raman spectroscopy more accessible.

AUTHOR CONTRIBUTIONS

Maarten Klaverdijk: Conceptualization; methodology; validation; formal analysis; investigation; software; writing—original draft; writing—review and editing; visualization. **Mehrab Nemati:** Investigation; software;

writing—review and editing. **Marcel Ottens**: Writing—review and editing; supervision. **Marieke E. Klijn**: Conceptualization; resources; writing—original draft; writing—review and editing; supervision; administration; funding acquisition.

ACKNOWLEDGMENTS

We would like to thank Christiaan Mooiman and Jeroen Schmidt for their technical support while setting up the lab and during the fermentations.

FUNDING INFORMATION

This project is funded by the Department of Biotechnology at Delft University of Technology.

CONFLICT OF INTEREST STATEMENT

The authors report no conflict of interest.

DATA AVAILABILITY STATEMENT

The data that support the findings of this study are available from the corresponding author upon reasonable request.

ORCID

Maarten Klaverdijk https://orcid.org/0009-0000-7744-8901

REFERENCES

1. FDA. *Guidance for industry: PAT—A framework for innovative pharmaceutical development, manufacturing, and quality assurance*. Food and Drug Administration; 2004.
2. Esmonde-White KA, Cuellar M, Uerpmann C, Lenain B, Lewis IR. Raman spectroscopy as a process analytical technology for pharmaceutical manufacturing and bioprocessing. *Anal Bioanal Chem*. 2017;409(3):637-649.
3. Rathore A, Bhambure R, Ghare V. Process analytical technology (PAT) for biopharmaceutical products. *Anal Bioanal Chem*. 2010;398(1):137-154. doi:10.1007/s00216-010-3781-x
4. Hirsch E, Pataki H, Domján J, et al. Inline noninvasive Raman monitoring and feedback control of glucose concentration during ethanol fermentation. *Biotechnol Prog*. 2019;35(5):e2848. doi:10.1002/btpr.2848
5. Pelletier MJ. Quantitative analysis using Raman spectrometry. *Appl Spectrosc*. 2003;57(1):20A-42A.
6. Esmonde-White KA, Cuellar M, Lewis IR. The role of Raman spectroscopy in biopharmaceuticals from development to manufacturing. *Anal Bioanal Chem*. 2021;414(2):969-991. doi:10.1007/s00216-021-03727-4
7. Metcalfe GD, Smith TW, Hippler M. On-line analysis and in situ pH monitoring of mixed acid fermentation by Escherichia coli using combined FTIR and Raman techniques. *Anal Bioanal Chem*. 2020;412:7307-7319.
8. Ryabchykov O, Guo S, Bocklitz T. Analyzing Raman spectroscopic data. *Phys Sci Rev*. 2019;4(2):20170043.
9. Bocklitz T, Walter A, Hartmann K, Rösch P, Popp J. How to preprocess Raman spectra for reliable and stable models? *Anal Chim Acta*. 2011;704(1–2):47-56.
10. Lieber CA, Mahadevan-Jansen A. Automated method for subtraction of fluorescence from biological Raman spectra. *Appl Spectrosc*. 2003;57(11):1363-1367.
11. Sinfield JV, Monwuba CK. Assessment and correction of turbidity effects on Raman observations of chemicals in aqueous solutions. *Appl Spectrosc*. 2014;68(12):1381-1392.
12. Shaw AD, Kaderbhai N, Jones A, et al. Noninvasive, on-line monitoring of the biotransformation by yeast of glucose to ethanol using dispersive Raman spectroscopy and chemometrics. *Appl Spectrosc*. 1999;53(11):1419-1428.
13. Müller DH, Flake C, Brands T, Koß HJ. Bioprocess in-line monitoring using Raman spectroscopy and indirect hard modeling (IHM): a simple calibration yields a robust model. *Biotechnol Bioeng*. 2023;120:1857-1868.
14. Jiang H, Xu W, Ding Y, Chen Q. Quantitative analysis of yeast fermentation process using Raman spectroscopy: comparison of CARS and VCPA for variable selection. *Spectrochim Acta A Mol Biomol Spectrosc*. 2020;228:117781.
15. Wang K, Chen J, Martiniuk J, et al. Species identification and strain discrimination of fermentation yeasts *Saccharomyces cerevisiae* and Saccharomyces uvarum using Raman spectroscopy and convolutional neural networks. *Appl Environ Microbiol*. 2023;89(12):e01673-23.
16. Iversen JA, Berg RW, Ahring BK. Quantitative monitoring of yeast fermentation using Raman spectroscopy. *Anal Bioanal Chem*. 2014;406(20):4911-4919. doi:10.1007/s00216-014-7897-2
17. Zakhartsev M, Reuss M. Cell size and morphological properties of yeast *Saccharomyces cerevisiae* in relation to growth temperature. *FEMS Yeast Res*. 2018;18(6):foy052.
18. Picard A, Daniel I, Montagnac G, Oger P. In situ monitoring by quantitative Raman spectroscopy of alcoholic fermentation by *Saccharomyces cerevisiae* under high pressure. *Extremophiles*. 2007;11(3):445-452.
19. Iversen JA, Ahring BK. Monitoring lignocellulosic bioethanol production processes using Raman spectroscopy. *Bioresour Technol*. 2014;172:112-120.
20. Domján J, Fricska A, Madarász L, et al. Raman-based dynamic feeding strategies using real-time glucose concentration monitoring system during adalimumab producing CHO cell cultivation. *Biotechnol Prog*. 2020;36(6):e3052. doi:10.1002/btpr.3052
21. Lee HL, Boccazzi P, Gorret N, Ram RJ, Sinskey AJ. In situ bioprocess monitoring of Escherichia coli bioreactions using Raman spectroscopy. *Vibr Spectrosc*. 2004;35(1–2):131-137.
22. Zhang S, Jia H, Song M, Shen H, Dongfei L, Haibo L. Raman spectroscopy study of acetonitrile at low temperature. *Spectrochim Acta A Mol Biomol Spectrosc*. 2021;246:119065.
23. Yoshikawa Y, Shigeto S. A simple calibration method of anti-stokes–stokes Raman intensity ratios using the water spectrum for intracellular temperature measurements. *Appl Spectrosc*. 2020;74(10):1295-1296.
24. Carey DM, Korenowski GM. Measurement of the Raman spectrum of liquid water. *J Chem Phys*. 1998;108(7):2669-2675.
25. Seki T, Chiang K-Y, Yu C-C, et al. The bending mode of water: a powerful probe for hydrogen bond structure of aqueous systems. *J Phys Chem Lett*. 2020;11(19):8459-8469.
26. Đuričković I, Marchetti M, Claverie R, Bourson P, Chassot J-M, Fontana MD. Experimental study of NaCl aqueous solutions by Raman spectroscopy: towards a new optical sensor. *Appl Spectrosc*. 2010;64(8):853-857.
27. Vogt F, Booksh K. Influence of wavelength-shifted calibration spectra on multivariate calibration models. *Appl Spectrosc*. 2004;58(5):624-635.
28. Seasholtz MB, Kowalski BR. Qualitative information from multivariate calibration models. *Appl Spectrosc*. 1990;44(8):1337-1348. doi:10.1366/000370290789619478
29. Wise BM, Roginski RT. A calibration model maintenance roadmap. *IFAC-PapersOnLine*. 2015;48(8):260-265.
30. Witjes H, Van den Brink M, Melssen W, Buydens L. Automatic correction of peak shifts in Raman spectra before PLS regression. *Chemometr Intell Lab Syst*. 2000;52(1):105-116.
31. Verduyn C, Postma E, Scheffers WA, Van Dijken JP. Effect of benzoic acid on metabolic fluxes in yeasts: a continuous-culture study on the regulation of respiration and alcoholic fermentation. *Yeast*. 1992;8(7):501-517.

32. Nijkamp JF, van den Broek M, Datema E, et al. De novo sequencing, assembly and analysis of the genome of the laboratory strain *Saccharomyces cerevisiae* CEN. PK113-7D, a model for modern industrial biotechnology. *Microb Cell Fact*. 2012;11(1):1-17. doi:10.1186/1475-2859-11-36
33. Pedregosa F, Varoquaux G, Gramfort A, et al. Scikit-learn: machine learning in python. *J Mach Learn Res*. 2011;12:2825-2830.
34. Lopez PC. Chemotools: a python package that integrates Chemometrics and scikit-learn. *Journal of Open Source Software*. 2024;9(100):6802.
35. Dudek M, Zajac G, Szafraniec E, et al. Raman optical activity and Raman spectroscopy of carbohydrates in solution. *Spectrochim Acta A Mol Biomol Spectrosc*. 2019;206:597-612. doi:10.1016/j.saa.2018.08.017
36. Padro JA, Martí J. An interpretation of the low-frequency spectrum of liquid water. *J Chem Phys*. 2003;118(1):452-453.
37. Walrafen G, Fisher M, Hokmabadi M, Yang WH. Temperature dependence of the low-and high-frequency Raman scattering from liquid water. *J Chem Phys*. 1986;85(12):6970-6982.
38. Sun Q. The Raman OH stretching bands of liquid water. *Vib Spectrosc*. 2009;51(2):213-217.
39. Ahmed M, Namboodiri V, Singh AK, Mondal JA, Sarkar SK. How ions affect the structure of water: a combined Raman spectroscopy and multivariate curve resolution study. *J Phys Chem B*. 2013;117(51):16479-16485.
40. Lednev VN, Grishin MY, Pershin SM, Bunkin AF. Quantifying Raman OH-band spectra for remote water temperature measurements. *Opt Lett*. 2016;41(20):4625-4628.
41. Thapa J, Liu B, Woodruff SD, Chorpening BT, Buric MP. Raman scattering in single-crystal sapphire at elevated temperatures. *Appl Optics*. 2017;56(31):8598-8606.
42. Matsumoto Y, Harada H, Yui K, Uchida H, Itatani K, Koda S. Raman spectroscopic study of aqueous alkali sulfate solutions at high temperature and pressure to yield precipitation. *The Journal of Supercritical Fluids*. 2009;49(3):303-309.
43. Rull F, Sobron F, Nielsen O. Dependence on concentration and temperature of the dynamics of SO in Li_2SO_4, Na_2SO_4 and K_2SO_4 aqueous solutions studied by Raman spectroscopy. *J Raman Spectrosc*. 1995;26(8–9):663-668.
44. Workman JJ Jr. A review of calibration transfer practices and instrument differences in spectroscopy. *Appl Spectrosc*. 2018;72(3):340-365.
45. Volger R, Puiman L, Haringa C. Bubbles and broth: a review on the impact of broth composition on bubble column bioreactor hydrodynamics. *Biochem Eng J*. 2024;201:109124.
46. Emmerich J, Tang Q, Wang Y, Neubauer P, Junne S, Maaß S. Optical inline analysis and monitoring of particle size and shape distributions for multiple applications: scientific and industrial relevance. *Chin J Chem Eng*. 2019;27(2):257-277.
47. Rudiš M, Jezdinský V, Štěrbáček Z. Physical properties of microbial suspensions: II. Properties of microbial suspensions and their supernatants during fermentation conditions. *Folia Microbiol*. 1977;22:128-133.
48. Mendelovici E, Frost RL, Kloprogge T. Cryogenic Raman spectroscopy of glycerol. *Journal of Raman Spectroscopy*. 2000;31(12):1121-1126.
49. Lange H, Heijnen J. Statistical reconciliation of the elemental and molecular biomass composition of *Saccharomyces cerevisiae*. *Biotechnol Bioeng*. 2001;75(3):334-344.
50. Czamara K, Majzner K, Pacia MZ, Kochan K, Kaczor A, Baranska M. Raman spectroscopy of lipids: a review. *J Raman Spectrosc*. 2015;46(1):4-20.
51. Rygula A, Majzner K, Marzec KM, Kaczor A, Pilarczyk M, Baranska M. Raman spectroscopy of proteins: a review. *J Raman Spectrosc*. 2013;44(8):1061-1076.
52. Hernández B, Pflüger F, Kruglik SG, Ghomi M. Characteristic Raman lines of phenylalanine analyzed by a multiconformational approach. *J Raman Spectrosc*. 2013;44(6):827-833.
53. Kochan K, Peng H, Wood BR, Haritos VS. Single cell assessment of yeast metabolic engineering for enhanced lipid production using Raman and AFM-IR imaging. *Biotechnol Biofuels*. 2018;11:1-15.
54. Yang N, Guerin C, Kokanyan N, Perré P. In-line monitoring of bioreactor by Raman spectroscopy: direct use of a standard--based model through cell—scattering correction. *J Biotechnol*. 2024;396:41-52.
55. Webster TA, Hadley BC, Hilliard W, Jaques C, Mason C. Development of generic raman models for a GS-KOTM CHO platform process. *Biotechnol Prog*. 2018;34(3):730-737. doi:10.1002/btpr.2633
56. Wieland K, Masri M, von Poschinger J, Brück T, Haisch C. Non-invasive Raman spectroscopy for time-resolved in-line lipidomics. *RSC Adv*. 2021;11(46):28565-28572.

SUPPORTING INFORMATION

Additional supporting information can be found online in the Supporting Information section at the end of this article.

How to cite this article: Klaverdijk M, Nemati M, Ottens M, Klijn ME. Impact of bioreactor process parameters and yeast biomass on Raman spectra. *Biotechnol. Prog*. 2025;e70050. doi:10.1002/btpr.70050